DOE/PC/30297-T3

ASSESSMENT OF PULVERIZED-COAL-FIRED COMBUSTOR PERFORMANCE

Second Quarterly
Technical Progress Report

W. Richter
W. Clark
R. Payne

Energy and Environmental Research Corporation
8001 Irvine Boulevard
Santa Ana, CA 92705

April 1981

Prepared for Pittsburgh Energy Technology Center
Department of Energy

Under Contract No. DE-AC22-80PC30297

cp

DISCLAIMER

TABLE OF CONTENTS

1.0 INTRODUCTION AND SCOPE

The objective of this program is to provide the engineering tools necessary for an authoritative assessment of the performance of industrial furnaces firing pulverized coal. The program incorporates two experimental tasks and is constructed around an analytical task (Task 1) which will identify and upgrade the family of computer programs required to undertake the performance analysis studies. These analytical tools will be used to predict the effect of parameters such as fuel type and furnace variables on combustor performance, and to identify those properties which have a major impact on thermal performance. The second task uses a combustion reactor to screen the key variables identified in Task 1 and to provide data on the properties of coal particulate matter which affect heat transfer performance. Verification of the engineering analytical approach will be provided by measurements made in a pilot-scale furnace in the third task.

This present report discusses technical progress during the second three months of the program effort (January-April 1981), and considers the selection, documentation, and modification of the appropriate analytical tools and further details of the Task 2 experimental system. In this reporting period details of the computer programs for the performance of analytical studies have been documented and presented in an interim report.

2.0 MODEL IMPROVEMENT AND ENGINEERING ANALYSIS (TASK 1)

During the first quarter of 1981, efforts on Task 1 of the project have been directed towards:

- An analytical tool verification for the planned combustor analysis, including the documentation and supply of test examples of three different mathematical combustor models.
- Upgrading work concerning one of these models, namely the rectangular furnace model.
- A preliminary study of the influence of submicron particles on radiative heat transfer.

2.1 Analytical Tool Verification

As described in the First Quarterly Report of the present project,[1] three different mathematical models have been chosen from available codes to serve as basic analytical tools for an engineering assessment of the behavior of p.f.-fired furnaces. These models are

- a 3D model of rectangular furnaces,
- a 2D model of cylindrical furnaces,
- a 2D elliptic flame model.

The first two models are decoupled, pure heat transfer models. They are based on a so-called semistochastic method[2] for computation of radiative interchange within a flexible arrangement of macro-sized furnace zones. The radiative exchange calculation is carried out for given distributions of temperatures and radiative properties within the furnace. However, the temperature field can also be calculated by means of a total energy balance of furnace zones. For this purpose, the flow and heat release pattern has to be prescribed throughout the furnace and net convective, diffusive, and radiative heat fluxes of each furnace zone, with originally unknown temperature, are equated to the net zonal release of chemically-bound heat. The resulting heat balance equations are iteratively solved. The radiative exchange calculation is repeated for each improved set of zonal temperatures until final convergence is achieved. Such a total energy balance has already been embodied in the rectangular furnace model and will be coded for the cylindrical furnace model in such a way that both models differ only in terms of the

geometry (i.e. in the type of co-ordinates used and in handling of furnace symmetries). The third model chosen as a tool for analysis of combustor performance is a 2D-coupled fluid flow, combustion and heat transfer model for axisymmetric gas and coal flames burning in cylindrical furnaces. The model includes submodels of turbulent exchange, homogeneous and heterogeneous flame reactions, kinetically- or mixing-controlled burnout and radiative transfer. In the finite-difference code, appropriate balance equations of mass, momentum, matter, and energy are simultaneously solved for so-called control volumes of an "Eulerian" coordinate system, yielding velocity, concentration, temperature, and heat flux distributions throughout the furnace. Since the control volumes of the finite-difference solution scheme are usually smaller than the zones of the pure-heat transfer models described above, a better local resolution of the heat transfer variables of the furnace is achieved with the former method. However, besides the complicated and expensive solution process, the coupled flame model suffers still from substantial uncertainties connected with the various submodels of physical and chemical processes mentioned above. This is especially true for the multidirectional radiative heat transfer which is only coarsely approximated by so-called 2- or 4-flux methods. However, as experienced in the past, the flame model can generate at least qualitatively correct recirculating flow and heat release pattern for enclosed flames. Thus, it will predominantly be used during the present project to demonstrate the coupling of a code for reacting flows with the cylindrical heat transfer furnace model which is advanced with respect to the computation of radiative exchange.

The two furnace models and the flame model are documented in a special topical report, "Models for Coal Combustor Performance-Analytical Tool Verification," delivered to DOE.[3] This documentation, together with the preparation of suitable test computations, has been the main effort of Task 1 during the first quarter of 1981. The contents of the report are summarized in the following:

Since no earlier documentation was available, the rectangular furnace model has been documented in full detail with emphasis on the semistochastic radiation model. In this model, the radiative interchange between furnace zones is simulated by emission and tracing of a finite number of beams. The method is similar to Monte Carlo approaches of radiant heat transfer; however,

certain events in a beam's history are deterministically evaluated from geometrical or physical laws instead of approximating these laws with uniform or weighted random numbers. The report shows how the total number of beams, as well as beam distributing parameters, influence the accuracy of predicted overall radiant heat transfer and local radiant heat fluxes. Also shown is how the accuracy of local heat flux predictions can be increased for a given number of beams by random angular shifting of individual bundles of beams (see also section 2.2.1 of the present report). The parametric study concerning the accuracy as well as sample calculations of the complete rectangular furnace model has been carried out for a fictional 5 x 5 x 15m methane-fired combustion chamber of a medium-sized, 117 MW_t utility boiler. The sample calculations which are supplied with complete input data demonstrate the influence of three different approaches of flow and heat-release pattern on temperature and heat-flux distributions in the combustion chamber and on the furnace efficiency. The systems studied were a well-stirred system with uniform heat release, a plug-flow system with local flame zones on the bottom of the furnace and a combined recirculation-flow/plug-flow system with flame zones raised with respect to the furnace bottom.

The description of the cylindrical furnace model is restricted to departures from the rectangular furnace model due to the handling of axisymmetry and due to different stages of development of both models. Since the available cylindrical code does not yet include total heat balances for furnace zones, the presented sample calculations of the cylindrical furnace model have been carried out with prescribed zonal temperatures. Two test examples have been supplied. One example deals with the computation of gray radiation exchange in a long cylindrical furnace with idealized temperature distribution. Radiative heat fluxes predicted for this test case are compared to predictions obtained for a radiation model which is based on exchange coefficients for zone pairs and was independently developed elsewhere.[4] As a second example, radiative transfer is predicted for a cylindrical furnace fired with a luminous heavy fuel oil flame. Model input data, especially the distributions of temperatures and radiative species, were taken from a flame trial carried out in an experimental, cylindrical, vertical, water-cooled, 1 MW furnace, operated at Stuttgart University.[5] Results of the radiative exchange calculation which included the effect of soot particles are compared to calorimetric measurements and to readings of a hemispherical radiometer.

The 2D elliptic-flame model is documented for the version developed to predict the behavior of bituminous high-volatile coal flames. Sample calculations with this model are supplied for two long, nonswirling 2.1 MW flames of a recent p.f. trial carried out by the International Flame Research Foundation (IFRF) for EPA under subcontract from EER.[6] A major problem of this part of the analytical tool verification consisted of modeling the complicated nonaxisymmetric boundary conditions of the test furnace which has been investigated with the present model for the first time. During this effort, the model could be extended to handle the effect of ash deposit layers at cooling tubes which are placed in front of refractory walls on overall and local heat transfer in the furnace and on the flame behavior. The two investigated flames differed by the ratio of secondary air to primary air velocity and by the primary air amount, i.e. the particle loading of the fuel jet. The overall agreement between measured and computed distributions of velocity, burnout, temperature, and other flame variables has been found satisfactory. The predictions reflect especially one principal difference between the measured behavior of the two investigated flames correctly; namely, that ignition of the flame with the lower amount of primary air occurred at the jet edges, whereas the flame with the higher amount of primary air ignited on the furnace axis. Major local discrepancies between computed and experimental values of flame variables are attributed to the simple one-step devolatilization model.

2.2 Upgrading Work for the Rectangular Furnace Model

The rectangular furnace model as described in the topical report, Ref. 3, has been upgraded with respect to the following points:

- Increase of accuracy of the radiation model in the case of higher optical thickness.
- Handling of furnace geometries with inclined walls.
- Incorporation of simple models of particulate radiation.

2.2.1 Improvement of Accuracy of Radiative Heat Flux Predictions for Higher Optical Thickness

The accuracy of the semistochastic radiation model described in Ref. 3 is dependent on the optical thickness, or for a given furnace geometry on the absorption coefficient K_a. For the same number of beams, the accuracy of the overall radiative heat transfer predictions decreased with increasing optical

thickness. This is due to the discrete starting points of beam bundles which were located in the geometric center of cells of the emitting zones (Figure 2-1b and 2-1c). The accuracy of the predicted heat transfer became especially poor when a weighted gray-gas approach was used to account for nongrayness of radiation. This is shown in Figure 2-2 (curves b ÷ d) where total emissivities computed with a 1-clear/2-gray-gas approximation approximation[7] for the methane-fired boiler combustion chamber (see Ref. 3) are plotted versus the total number of beams which simulate the radiative exchange in the furnace enclosure. The poor accuracy is caused by the fact that one of the three gray gases had a very high absorption coefficient as is usually found in approximations of this type. Computation of radiative exchange in this gray gas would normally require a diffusion approach;[8] however, a significant improvement of the predictions with the present method (curve a, Figure 2-2) could be achieved by random shifting of starting points of individual beams of a bundle within a cell as shown in Figure 2-1e.

The introduction of a random shifting of starting points within cells, and of random orientation of beam bundles of different volume cells as already described in Ref. 3 inevitably increased the statistical error. However, this error is less than that produced by complete random choice of both beam direction and starting points as would be found in a pure Monte Carlo approach (Figure 2-1a). This is illustrated in Figure 2-3b where the statistical error of local heat flux at the top and bottom wall of the gray radiating combustion chamber (5 x 5 x 15m, K_a = 0.0893 1/m, ε = 0.8) obtained for the semistochastic distribution of beams (curves b, c, and d) is compared to the error obtained for pure random beam distribution (curve a). The statistical error shown by curve a would be further increased if absorption had also been treated on a random basis. The decrease in statistical error due to the use of the semistochastic method is not achieved at the expense of an increase in systematic error since even at lower beam numbers the mean values of predicted heat fluxes approximate the "exact" value (see Figure 2-3a).

2.2.2 Handling of Furnace Geometries With Inclined Walls

For the furnace model to be of engineering value it must be able to handle, without undue increase in computational time, practical geometries which normally include inclined walls on two planes. In order to account for such shapes, the code for emission as well as for beam tracing has been modified.

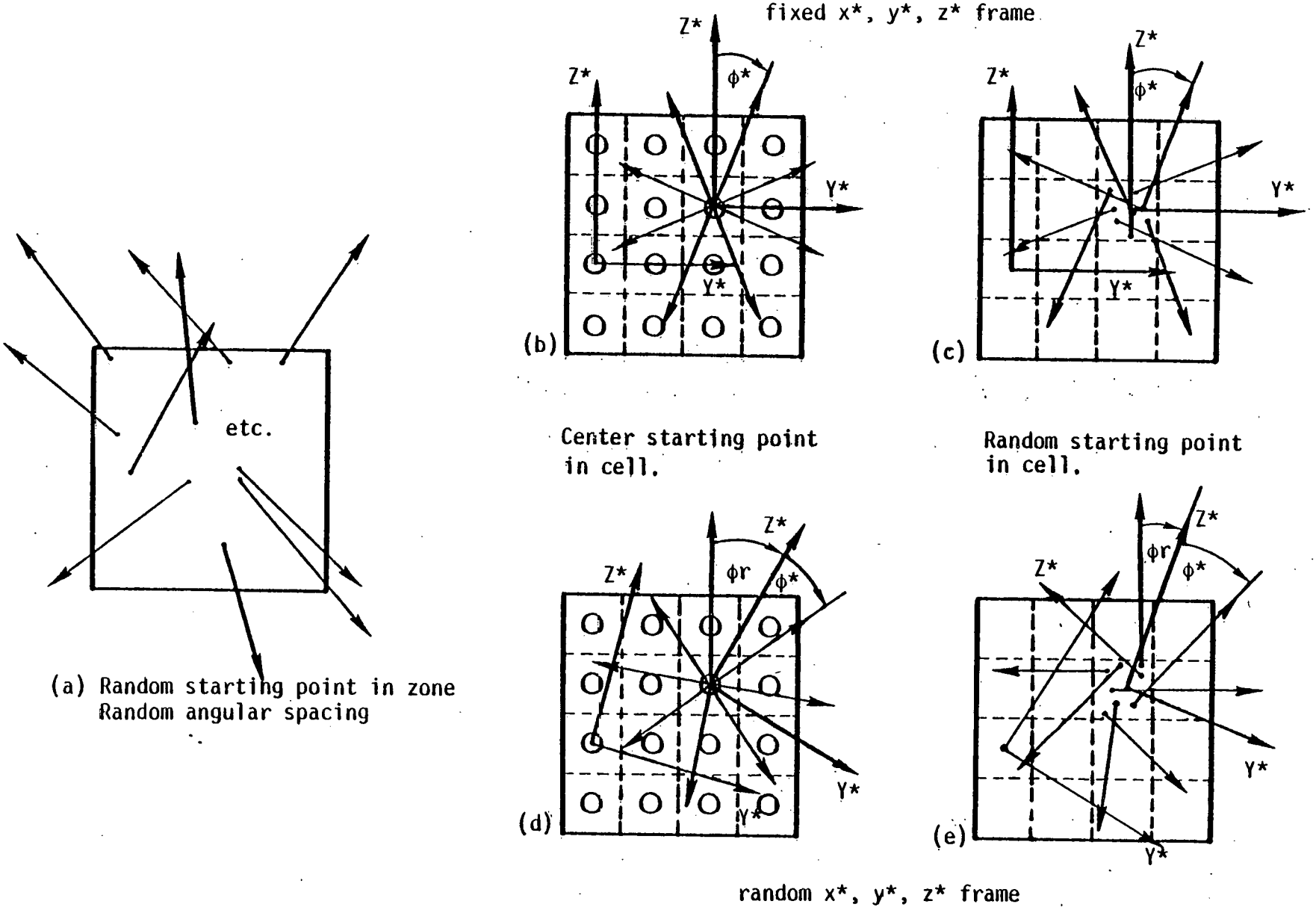

Figure 2-1. Distribution of Beams with Random Angular Spacing (a) and with Fixed Angular Spacing (b-e).

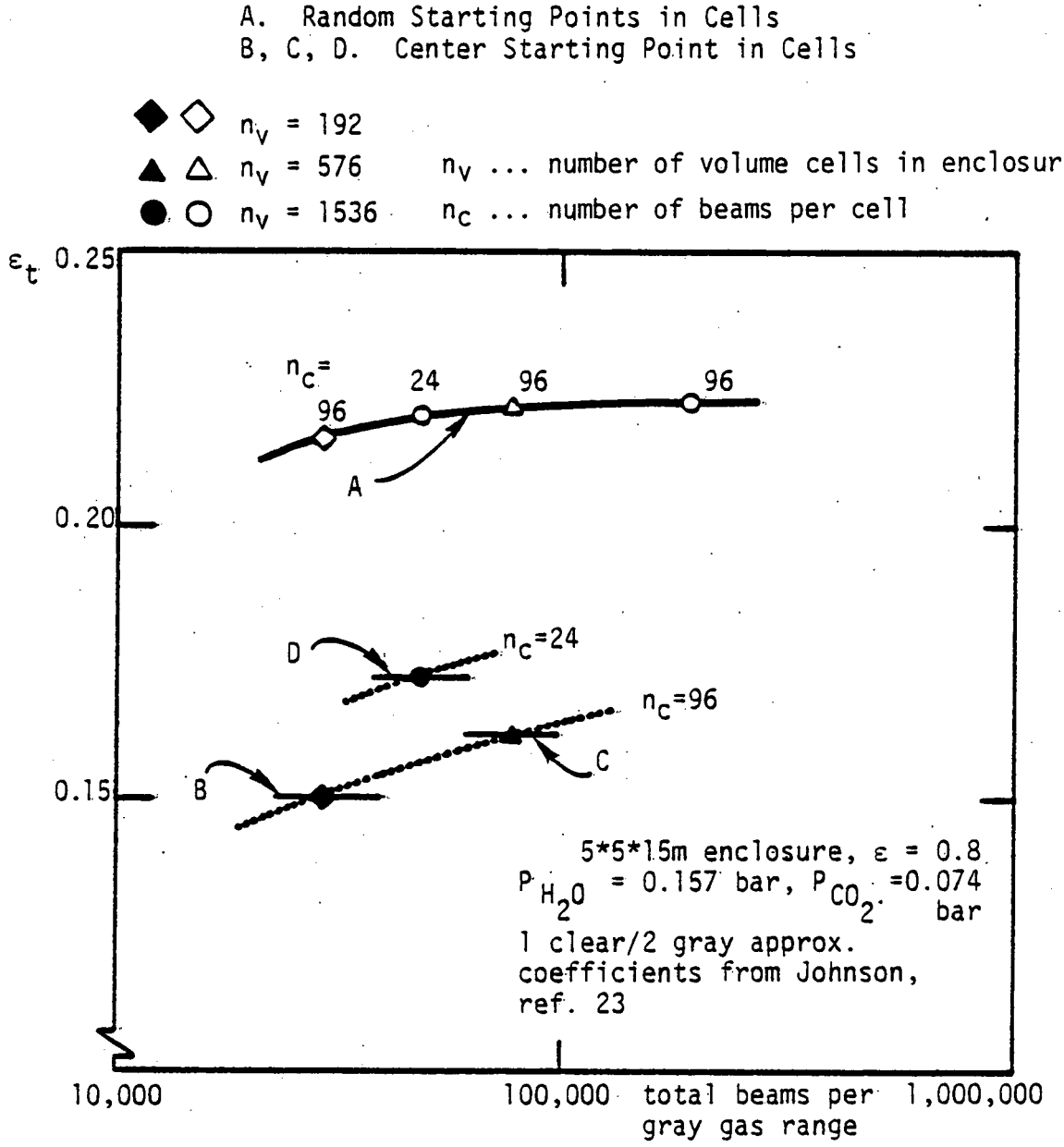

Figure 2-2. Total Emissivity ε_t with 1 Clear/2 Gray Gas Approximation Dependent on Total Number of Beams.

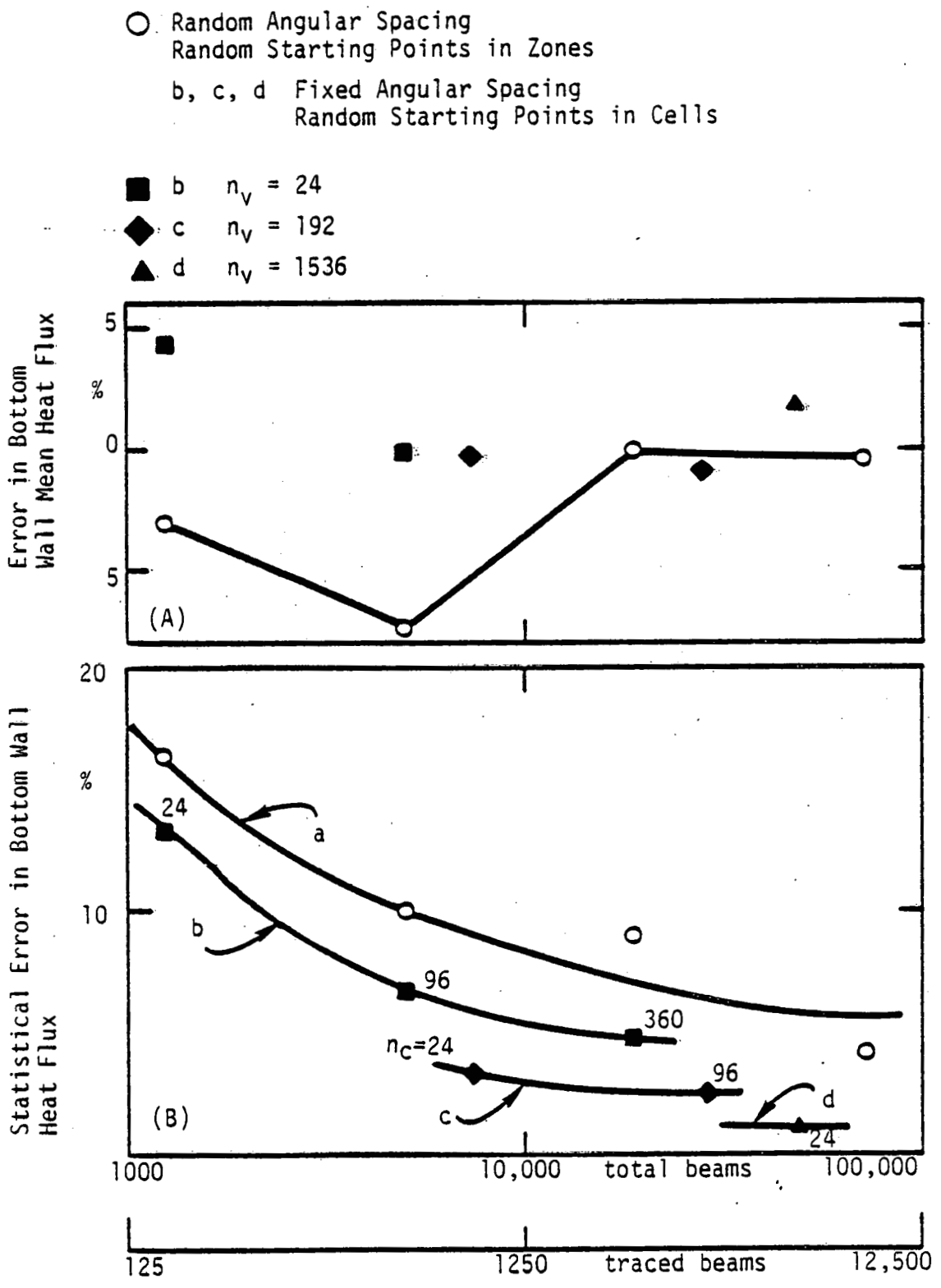

Figure 2-3. Error of Mean Value (A) and Statistical Error (B) of Computed Heat Fluxes of Bottom Wall Zones.

The coding of emission of arbitrarily prismatic zones is similar to that developed for the rectangular zones in a cartesian arrangement. According to Figure 2-4, a prismatic zone V_I is enclosed by the smallest possible parallelepiped $V_{I,p}$ with respect to the x, y, z frame. V_I and $V_{I,p}$ have otherwise the same properties. The distribution of the emitted energy flux $\dot{Q}_{e,I,p}$ of the parallelepiped into beams follows the algorithm described in Ref. 3 with the only restriction that the option of random distribution of starting points within a cell is applied (Figure 2-1c or 2-1e). Beams with starting points outside V_I are not traced and, therefore, in order to obey the energy balance of the prismatic zone their energy fluxes $\Delta\dot{Q}_{I,o}$ are subtracted from $\dot{Q}_{e,I,p}$. Thus, the emitted and traced energy flux finally approaches the one of the prismatic zone $\dot{Q}_{e,I}$. The logistics of beam tracing in the arrangement of prismatic zones is the same as for the rectangular zone arrangement; however, the path length Δs within the prismatic zones has to be computed by relatively complicated trigonometric relations from a knowledge of the coordinates of each edge point of the entered zone. In principle, if the coordinates of edge points of all zones and the relevant zonal properties are supplied as input data, the present code can predict radiative exchange in zone arrangements very similar to "finite element" structures. When a predominantly rectangular zone system is required, zone meshes for complex furnace geometries are generated automatically from a knowledge of the edge points of the furnace contour.

A test computation with the extended code was carried out for a methane-fired boiler operated as listed in Table 2-1. However, the rectangular furnace shape was replaced by a more complex geometry with ash hopper and nose as it is shown in Figure 2-5 together with the considered heat release and recirculating-flow pattern. The influence of this new geometric arrangement on both temperatures and heat flux distribution is revealed in Figures 2-6a and 2-6b, respectively. The increased temperatures in the lower half of the furnace with the ash hopper can be attributed to a reduction in both the radiating volume and in the cold-surface area in the lower furnace zones, compared to the rectangular furnace. The impact of the furnace nose on temperatures and heat flux distribution in the upper part of the furnace is significant. The shadow effect of the nose, in combination with the assumed recirculating pattern, gives lower temperatures in the volume zones behind the nose, resulting in low heat fluxes to the neighboring surface zones. The calculated outlet

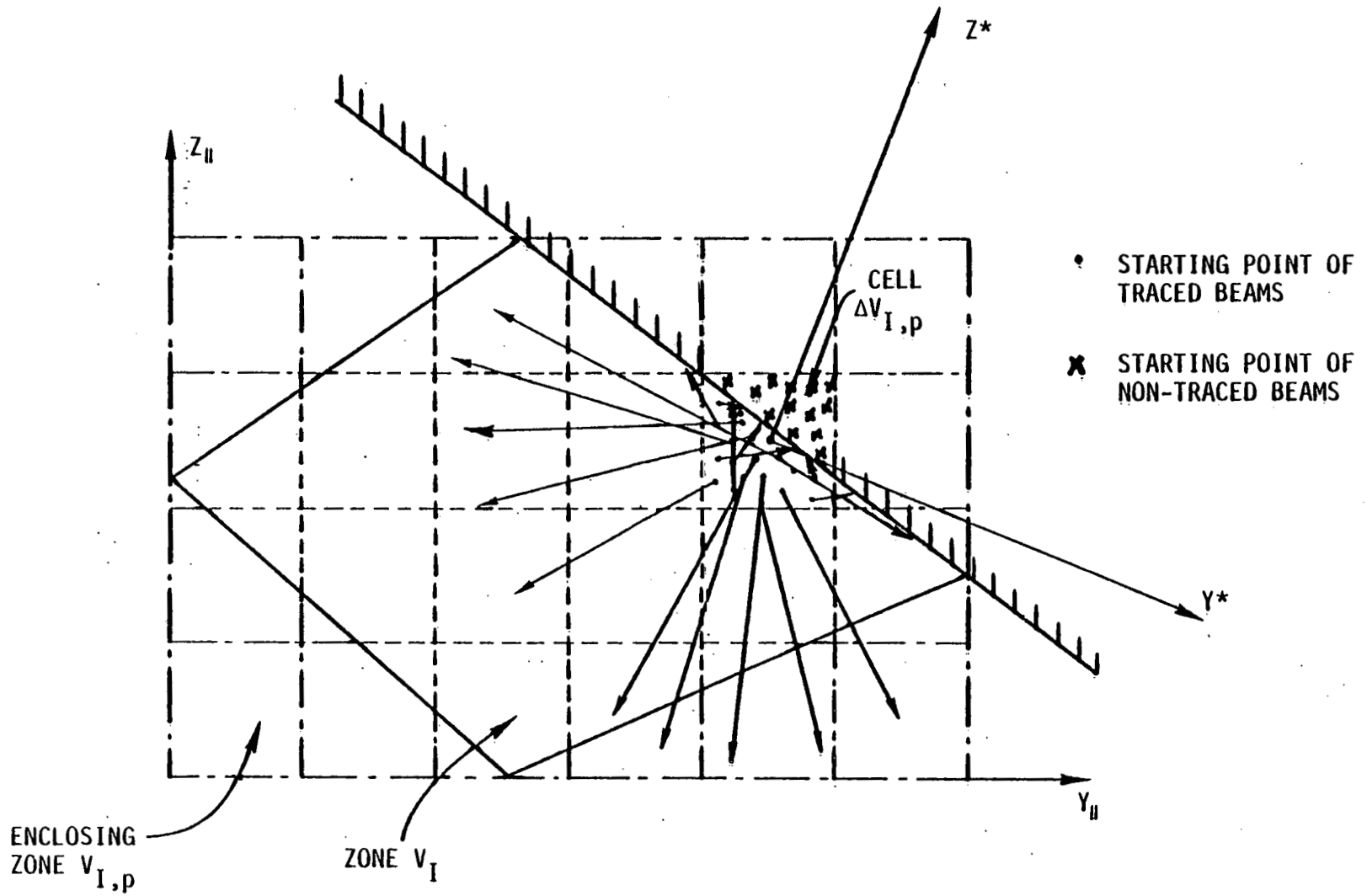

Figure 2-4. Handling of Emission of Beams From Arbitrary Prismatic Zones.

Table 2-1. Operating and Boundary Conditions of Modeled Boiler Combustion Chambers

	Gas-Fired Boiler	Coal-Fired Boiler
Furnace Geometry	5 x 5 x 15 m	
Fuel	CH_4 (sat'd at 289 K)	HVA Coal (1.4% moisture)
Lower Cal. Value	49961.6 kJ/kg_{dry}	31506 kJ/kg_{dry}
Thermal Input	117 MW	
Excess Air	30%(half sat'd at 289 K)	
Air Temperature	298 K	
Total Mass Flow $\dot{M}_o$	54.55 kg/s	55.50 kg/s
Fuel Mass Flow	2.34 kg_{dry}/s	3.71 kg_{dry}/s
Wall Temperature	700K	
Surface Emissivity	0.8	
Convective HT Coefficient	$\approx$0.0058 kW/m^2 K (see Ref. 9)	
Ambient Temperature	298 K	

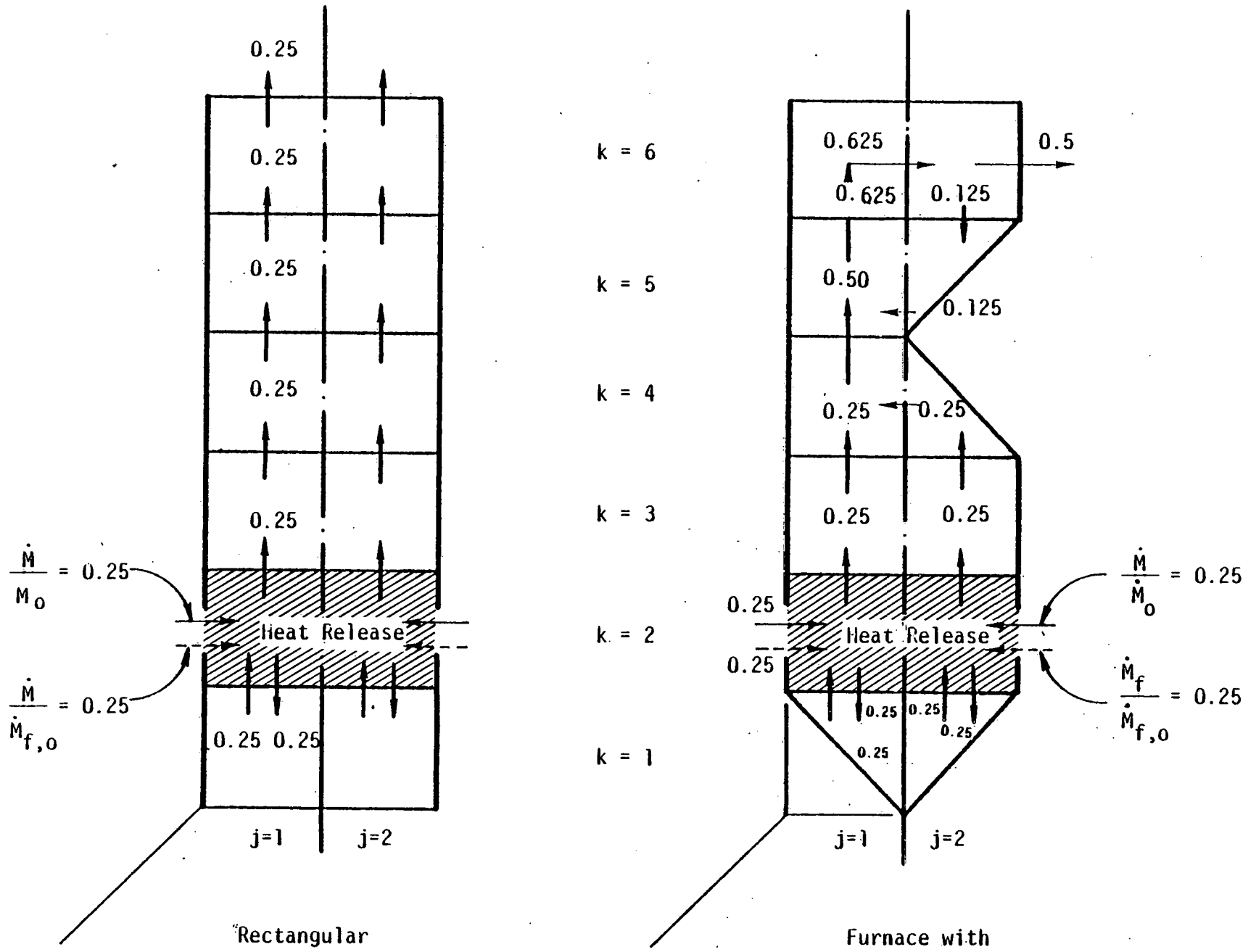

Figure 2-5. Assumed Flow and Heat Release Pattern for Boiler Combustion Chambers of Different Geometry.

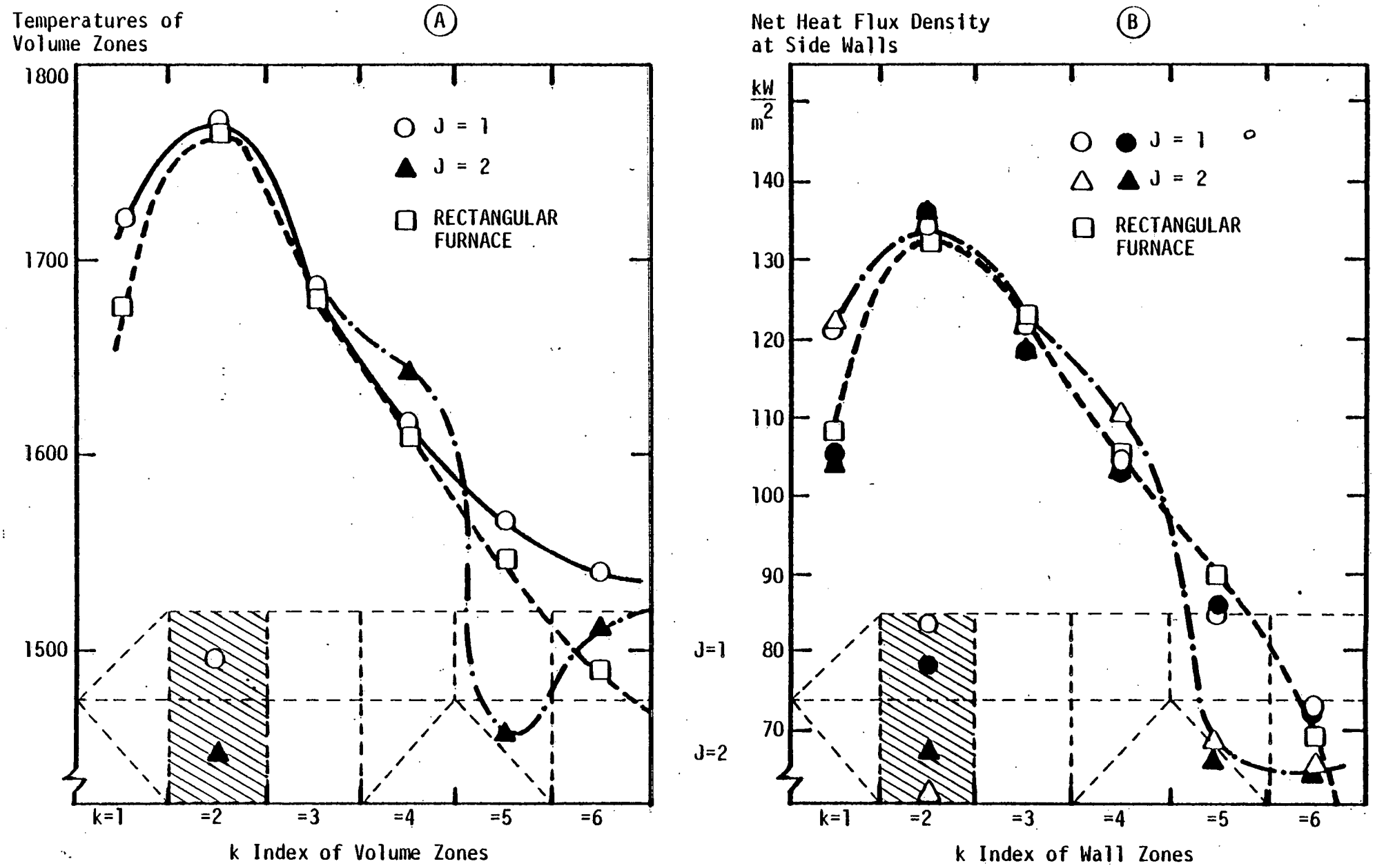

Figure 2-6. Effect of Furnace Geometry on Distribution of Temperature (A) and Heat Flux Density (B) in a Gas-Fired Boiler Combustion Chamber.

temperature for the nonrectangular furnace is approximately 30 K higher than that of the rectangular furnace. This is because the rectangular furnace has a 10 percent larger mean beam length and a 10 percent increase in cool surface area over the furnace with the ash hopper and nose.

2.2.3 Heat Transfer in a Coal-Fired Combustion Chamber

A preliminary study was carried out in order to test simple models of particulate radiation incorporated into the furnace model and in order to illustrate the impact of solid particles on the radiative transfer inside a coal-fired combustion chamber. The input data for the test example was similar to that used for the gas-fired rectangular combustion chamber mentioned above (Table 2-1 and Figure 2-5). However, the recirculating-mass flow rate was only half that of the input-mass flow rate, i.e. $\dot{M}_r = 0.5\ \dot{M}_o$. Figure 2-7 provides the properties of the high-volatile bituminous coal and the distribution of radiating species within the furnace zones. Four different conditions are identified. These are:

1. The total furnace volume is filled with the products of complete combustion.
2. The total furnace volume is filled with both the gaseous products and a uniform distribution of ash particles of mean diameter 16.8 μm. This corresponds to one ash particle per coal particle of 50 μm mean size (see Ref. 9).
3. In addition to 2 above, the heat release zone is assumed to contain char particles. The char concentration is one-tenth of the unburned coal particles, but has the same specific surface area as coal. A size distribution factor of 2.39 is chosen for both the char and ash particles.
4. The heat release zone was also assumed to contain soot particles, and their concentration was computed from a simple model described in Ref. 9. It was assumed that 10 percent of the original volatile carbon in the coal was converted to soot, with a mixing controlled reaction time of one-tenth of the residence time of the total furnace volume.

Radiation of the ash and char particles was assumed to be gray with a mean efficiency factor for absorption of 0.2 and 1, respectively. The radiative

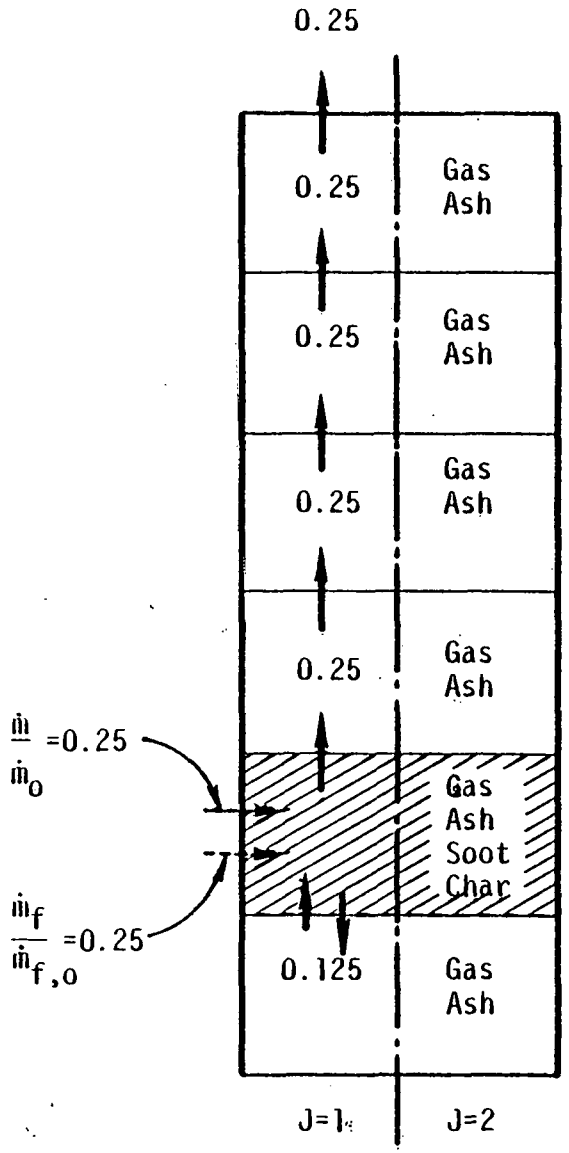

Properties of HVA Coal

C: 79.5%, H: 5.2%, O: 6.1%, S: 1.3%, N: 1.4% kg/kg dry

Ash: 6.5% kg/kg dry

Moisture: 1.4%

Low Cal. Val.: 31506 kJ/kg

Concentration of Species

Gas, Ash: Uniform (30% excess air)

Char: 1/10 of coal in heat release zone

Soot: 2% of C of coal (as fired), burning time 1/10 of furnace residence time

Modeling of Radiative Cloud Properties

Gas: 1 clear/2 gray

Ash: gray, X_a = 0.2, $\bar{x}$ = 16.8 μm, size distribution factor: 2.39

Char: gray, X_a = 1.0, specific surface area of coal ($\bar{x}_{coal}$ = 50 μm, size distribution factor: 2.39)

Soot: Johnson Model, 3 weighted gray gases

Figure 2-7. Assumptions for Computation of Radiative Heat Transfer in a Coal-Fired Combustion Chamber.

properties of the soot gas suspension were modeled with a three-weighted gray-gas approach suggested by Johnson.[7]

The impact of the presence of particulates on both the peak heat flux and the gas temperature distribution is shown in Figures 2-8a and 2-8b. Although the absolute value of these predictions is in doubt because of the assumptions used in the assessment of radiative properties and upon the particulate concentration, the results do illustrate the relative impact of particulate matter on thermal performance. In this case, the presence of particles can account for a variation of more than 100 K in the furnace outlet temperature, and the peak heat flux for the presence of char and soot in the heat release zone is approximately twice that which would be calculated assuming only gaseous radiation.

Further results of the impact of particles on the heat transfer in boilers as well as more details about the used models of particulate radiation may be found in Ref. 10.

2.3 Preliminary Study of Influence of Submicron Particles on Radiative Transfer

This study was carried out to supply Task 2 with information to enable a suitable choice of particulate analysis techniques. Although submicron particles are of major concern with respect to pollution it was thought that expensive, highly-sophisticated equipment for analyzing submicron particles would only be justified for the present project if submicron fly ash would significantly contribute to the radiative transfer. In order to generalize the data and to allow a comparison, the present preliminary study covered the influence of all possible submicron particles of p.f. combustion, namely ash, soot, coal, and char particles.

Results of the study are summarized in Table 2-2. One important quantity in the radiative behavior of particles is the complex refractive index of the particle material. There is little data concerning this index available in the literature, especially for the temperature range encountered in a p.f. combustor. Representative mean values tentatively concluded from a literature survey[9,11÷18] are listed in column 2 of Table 2-2 for the investigated species. For ash particles, also the minimum and maximum values of the refractive index found in literature are cited.

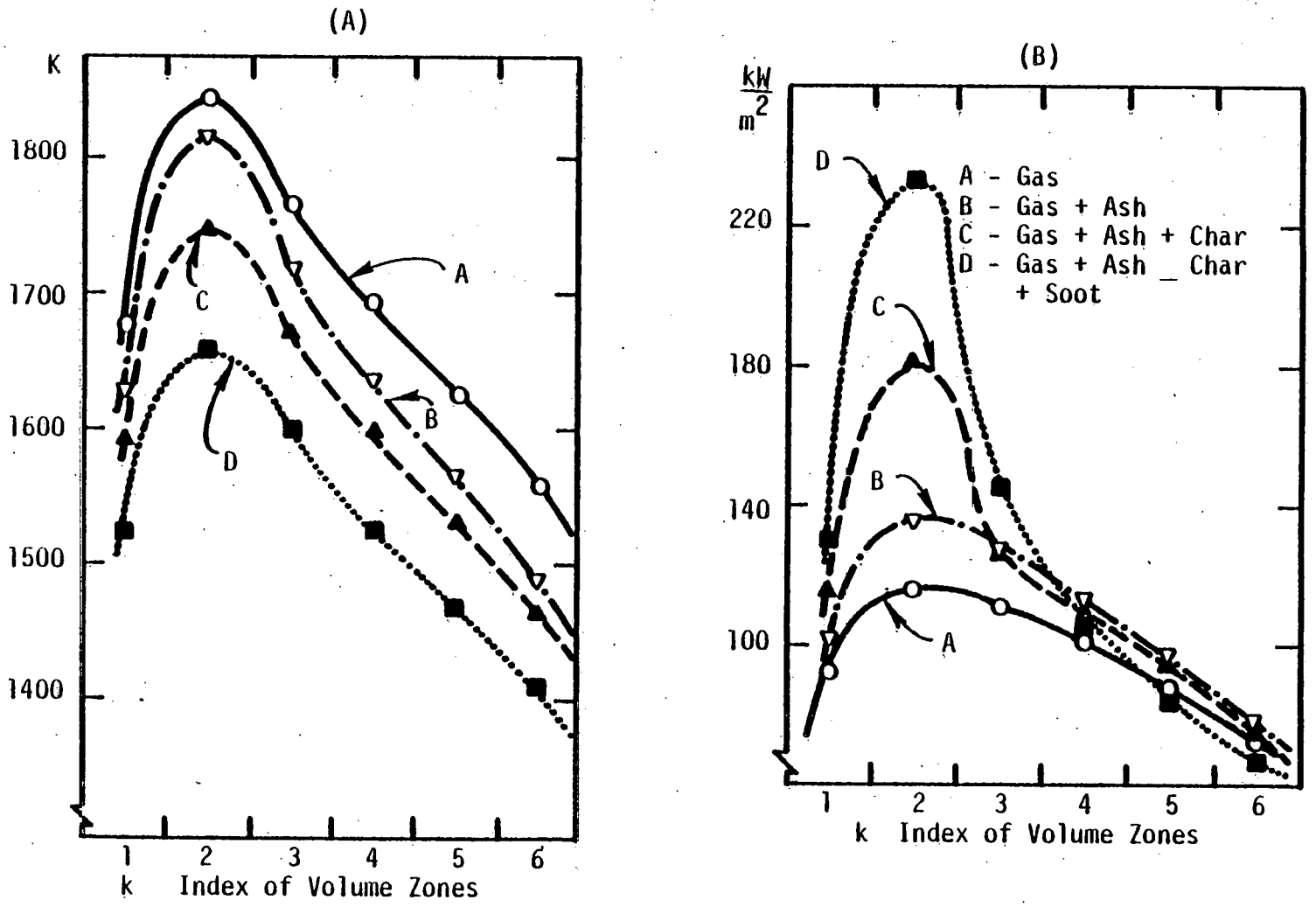

Figure 2-8. Effect of Particulates on Temperature Distribution (A) and Heat Flux Density at the Side Walls (B) in a Coal-Fired Boiler Combustion Chamber.

Table 2-2. Effect of Submicron Particulates ($c = 15.6 \cdot 10^{-6} kg/m^3$ at 1500 K) on Radiative Transfer in a 5 x 5 x 15m Combustion Chamber

Species	Complex Refractive Index	Constant a_o	Density of Material	Absorption Coefficient (Eq. 1)	Emissivity
	-	1/Km	kg/m^3	1/m	-
Ash	"mean": 1-50-0.020i	45.8	2300	0.0005	0.0018
	max: 1.50-1.000i	2111.5	"	0.0215	0.0795
	min: 1.50-0.005i	11.4	"	0.0001	0.0005
Soot	1.90-0.800i	1233.2	1000	0.0289	0.1053
Anthracite	2.00-0.600i	879.6	1300	0.0158	0.0592
Bituminous Coal	1.70-0.320i	621.5	1300	0.0112	0.0422
Char	1.93-1.020i	1447.7	900	0.0376	0.1351

For further simplification, it was assumed that the submicron particles can be represented by a 0.1 μm, monosized distribution (see also Ref. 19) and that thermal radiation is characterized by a mean wavelength according to $\overline{\lambda} \cdot T = 0.004107$ mK with T chosen at 1500 K. With these assumptions, the radiative behavior of the particles falls clearly into the Rayleigh regime of scattering, where the absorption efficiency of the particles can easily be computed from an approximate solution of the Mie equations.[8] It can be shown that the absorption coefficient of a particle cloud is given in that case by

$$K_a = a_o \, T \, \frac{c}{\rho} \quad 1/m \quad , \qquad (1)$$

where c is the particle concentration and ρ the density of the particle material (both in k_g/m^3). Values of the constants a_o (1/Km) for the different species are listed in column three of Table 2-2.

The concentration of submicron particles is assumed to be 15.6 mg/m^3 at 1500 K, which corresponds to a value measured in a coal-fired utility boiler (see Ref. 19) and which also would mean that about 1 ÷ 2 percent of the coal ash forms submicron particles by vaporization and condensation, if the submicron particles consist completely of fly ash. Using appropriate values of the density of particle material (column four), computed absorption coefficients of the different particle clouds are presented in column five of Table 2-2.

Finally, emissivities have been calculated with these absorption coefficients using a mean beam length $L_m = 3.6 \, V/A = 3.86$m corresponding to a 5 x 5 x 15m combustion chamber of a medium sized boiler (last column, Table 2-2). These emissivities should be compared to $\varepsilon \approx 0.3$ which is a representative emissivity of the volume of the combustion gases in this case. It can be concluded that if submicron particles are fly ash--as they are likely to be--, probably no important influence on radiative heat transfer can be expected. However, this depends very much on the concentration and on the optical constants of these particles, which may vary for different types of fuel and combustion conditions. For ash submicron particles also, maximum and minimum values of ε are recorded in Table 2-2 corresponding to the maximum and minimum values of the absorption index found in literature and demonstrating the uncertainty to which the present study is subjected.

3.0 REACTOR STUDIES (Task 2)

Efforts this quarter have been directed toward detailed design and construction of the reactor system and troubleshooting some of its components. Next quarter system assembly will be completed and the screening studies will begin.

The general objective of the reactor studies is to use a small-scale reactor, where coal combustion and the properties of particulate material can be studied under controlled conditions of temperature and gas composition, to provide information on those parameters which affect the thermal performance of coal-fired combustors. Figure 3-1 is a general schematic of the reactor system. Principal components include:

- Supply System
- Reactor System
- Measurement System
- Exhaust System

The following sections present further details of each of these component systems.

3.1 Supply System

The supply system includes the gas metering system and the coal-feed system. The gas metering system consists principally of Matheson rotameters and valves to monitor and control the flow of air, supplemental methane, and backfiring propane to the fluidized bed particle feeder, burner, and backfired reactor.

The coal feed system, shown schematically in Figure 3-2, consists of a fluidized-bed coal feeder based on a design suggested by Hamor and Smith[22] and a stream splitter. Gas is passed through a porous metal flow distributor into the narrow fluidizing zone at a sufficient velocity to fluidize the pulverized coal. Part of this gas, along with the entrained particles, flows into a small offtake tube. Carrier gas is added within the offtake tube, and transport gas is added at the exit of the offtake tube to prevent clogging. The stream splitter divides the total flow into five equal streams which supply the multiple injector burner. The bulk of the fluidizing gas bypasses the offtake tube and leaves the narrow fluidizing zone. It expands, slowing

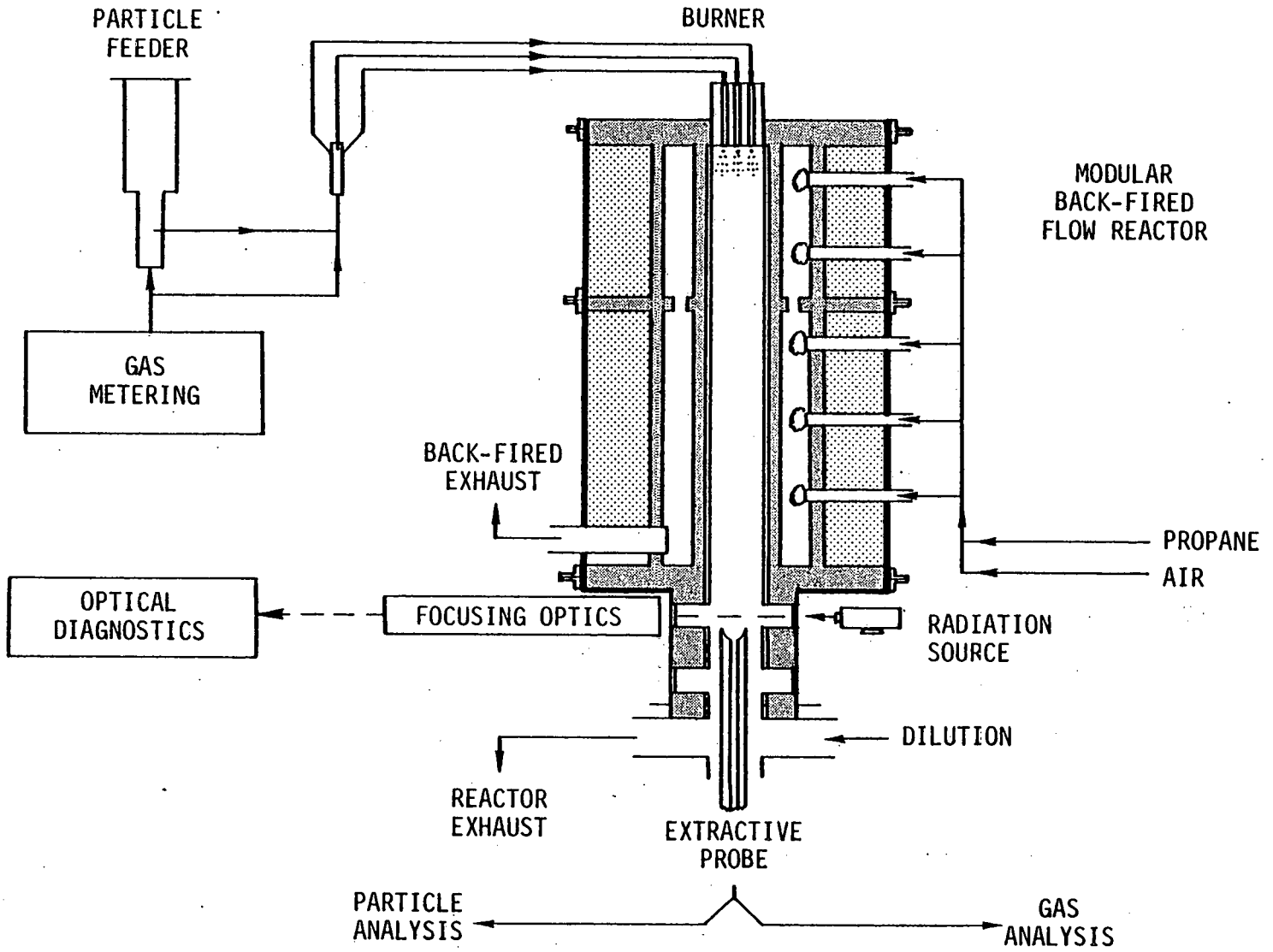

Figure 3-1. Reactor System.

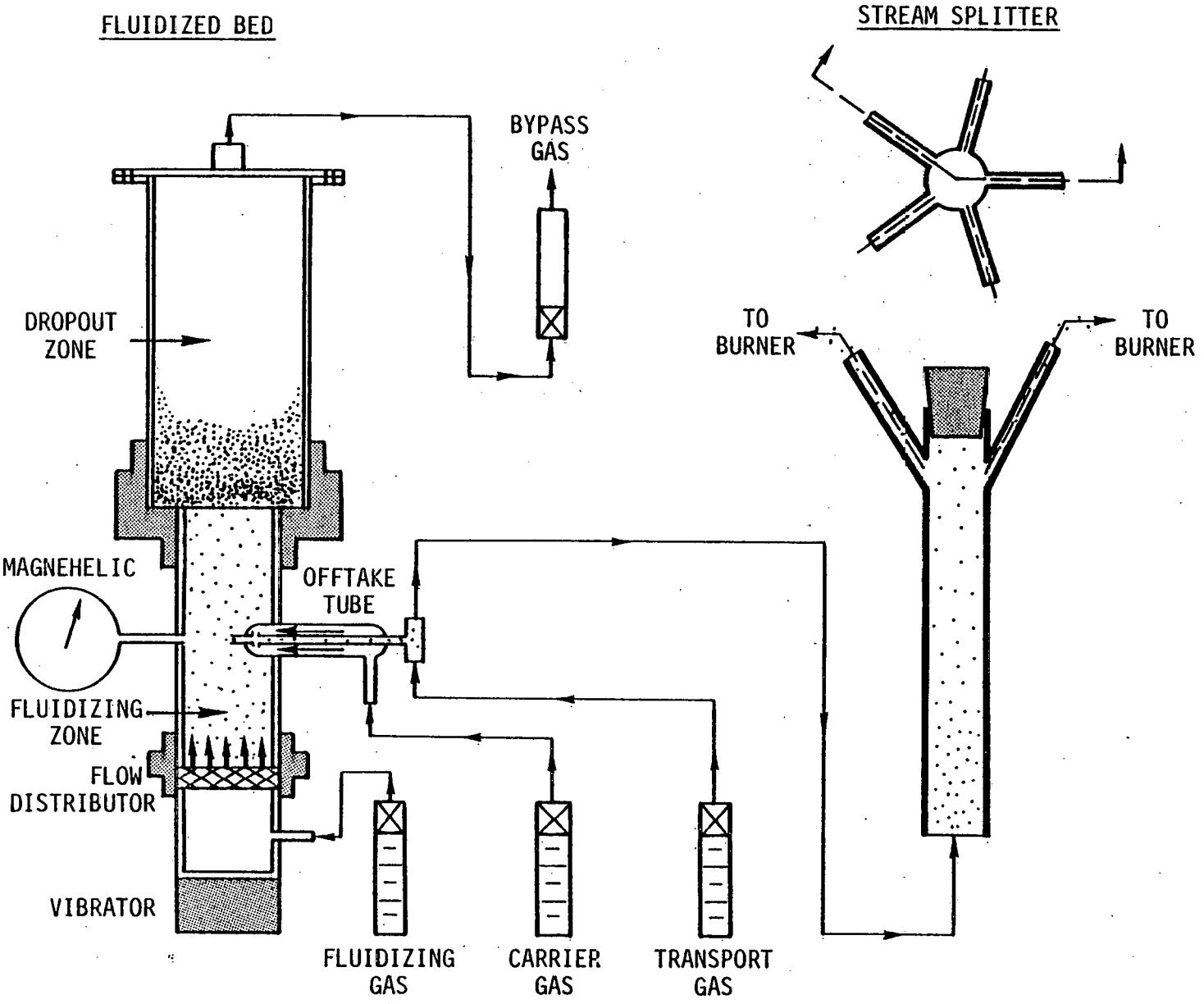

Figure 3-2. Coal Feed System.

down and dropping out the fluidized particles before leaving the top of the fluidized feeder. Coal feed rate increases with bed pressure (controlled by a valve on the bypass stream) and decreases with carrier gas flow as shown in Figure 3-3. Stream splitter tests indicate that under the same operating conditions the rate of particles flowing through the different splitter legs varies by less than 20 percent as shown in Figure 3-4. Calibrations are performed by weighing batch samples taken over a measured period of time.

3.2 Reactor System

The reactor system consists of burner, modular backheated reactor, and access module. The first of the burners to be tested is the multiple injector burner, shown in Figure 3-5. A cross pattern of five injectors is housed in a water-cooled can. Each injector consists of a central methane tube concentric within an outer coal/air tube. Swirl vanes impart tangential velocity to the coal/air streams, rapidly dispersing them to fill the combustion chamber. The independent methane stream, if used, tends to stabilize the flame and allows control of the adiabatic flame temperature. Visual observation of the burner operating against a cold background indicates that the multiple injector burner provides a stable flame over a wide range of methane/coal/air flows.

The backfired reactor consists of a series of modules of different lengths which can be used alone, or in conjunction to vary the residence time from 0 (no reactor) to 1.5 seconds, sufficient time for complete char burnout at intermediate temperatures. The interchangeable alumina flow tube has an inside diameter of 57 mm. Uniform, controlled backheating to 1650 C is achieved by backfiring the reactor with propane fired tangentially in alternating clockwise, counterclockwise directions. Temperatures are measured by type B thermocouples (platinum 6 percent rhodium vs. platinum 30 percent rhodium). The combustion chamber is lined with SALI low density, high strength insulation and the alumina flow tube is buffered from excessive thermal shock due to transient thermal gradients by a thin layer of the same material. The 30 cm diameter steel housing is flanged for ease of assembly, connecting on the inlet side to an adaptor for the burner, and on the outlet side to additional backfired modules or to the access module.

The access module is shown in Figure 3-6. It consists of a 51 mm square insulated flow chamber housed in a 127 mm square steel tube. Two

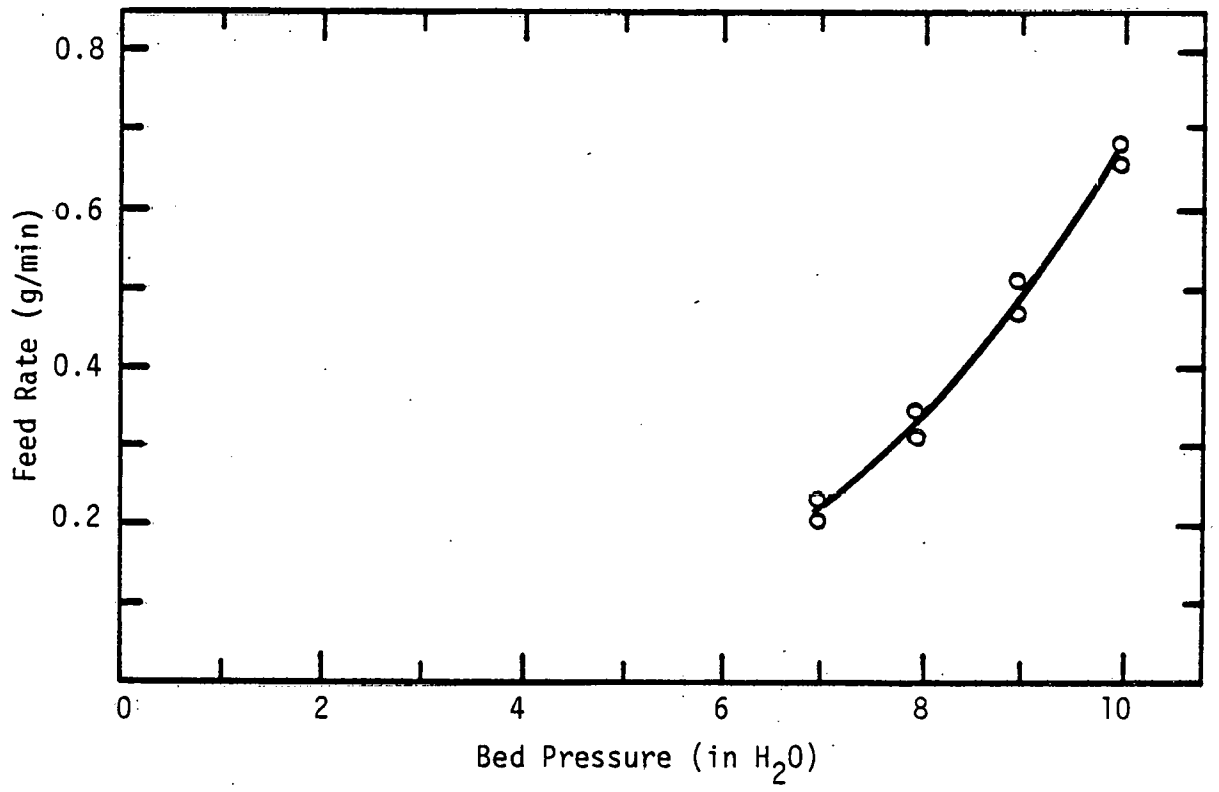

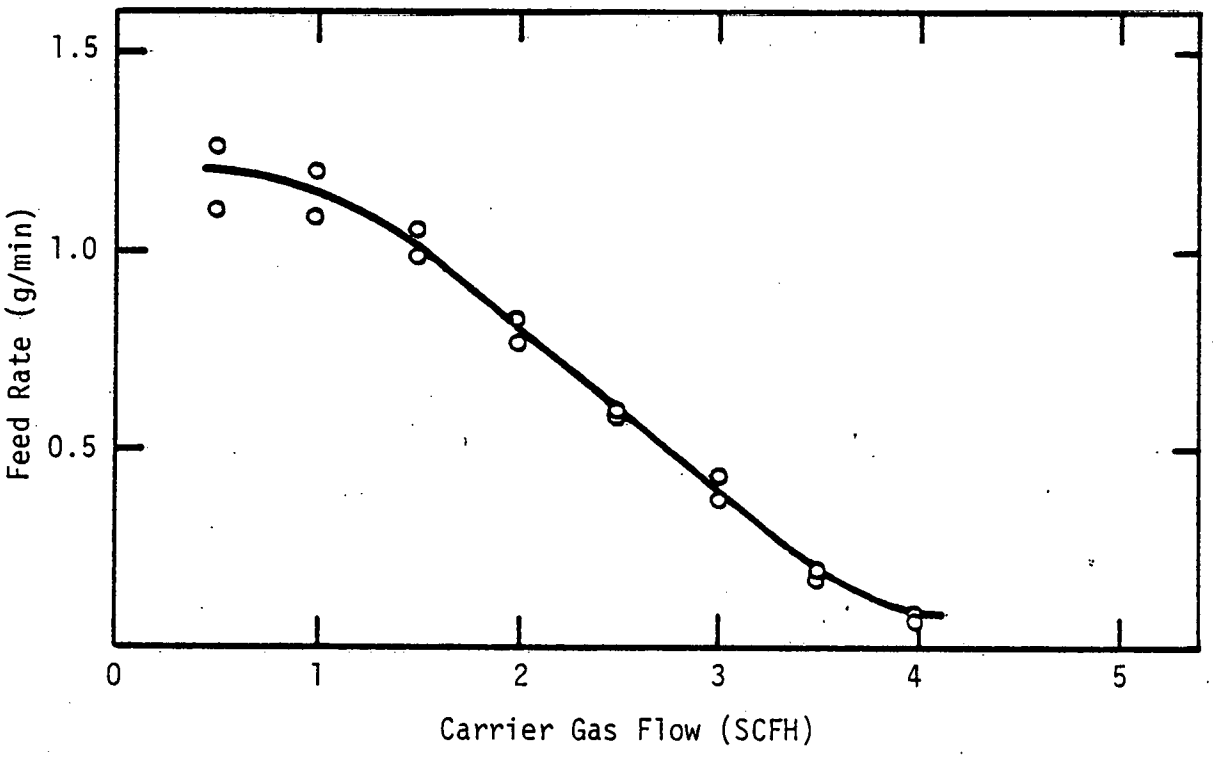

Figure 3-3. Effects of Bed Pressure and Carrier Gas Flow on Fluidized Bed Feed Rate.

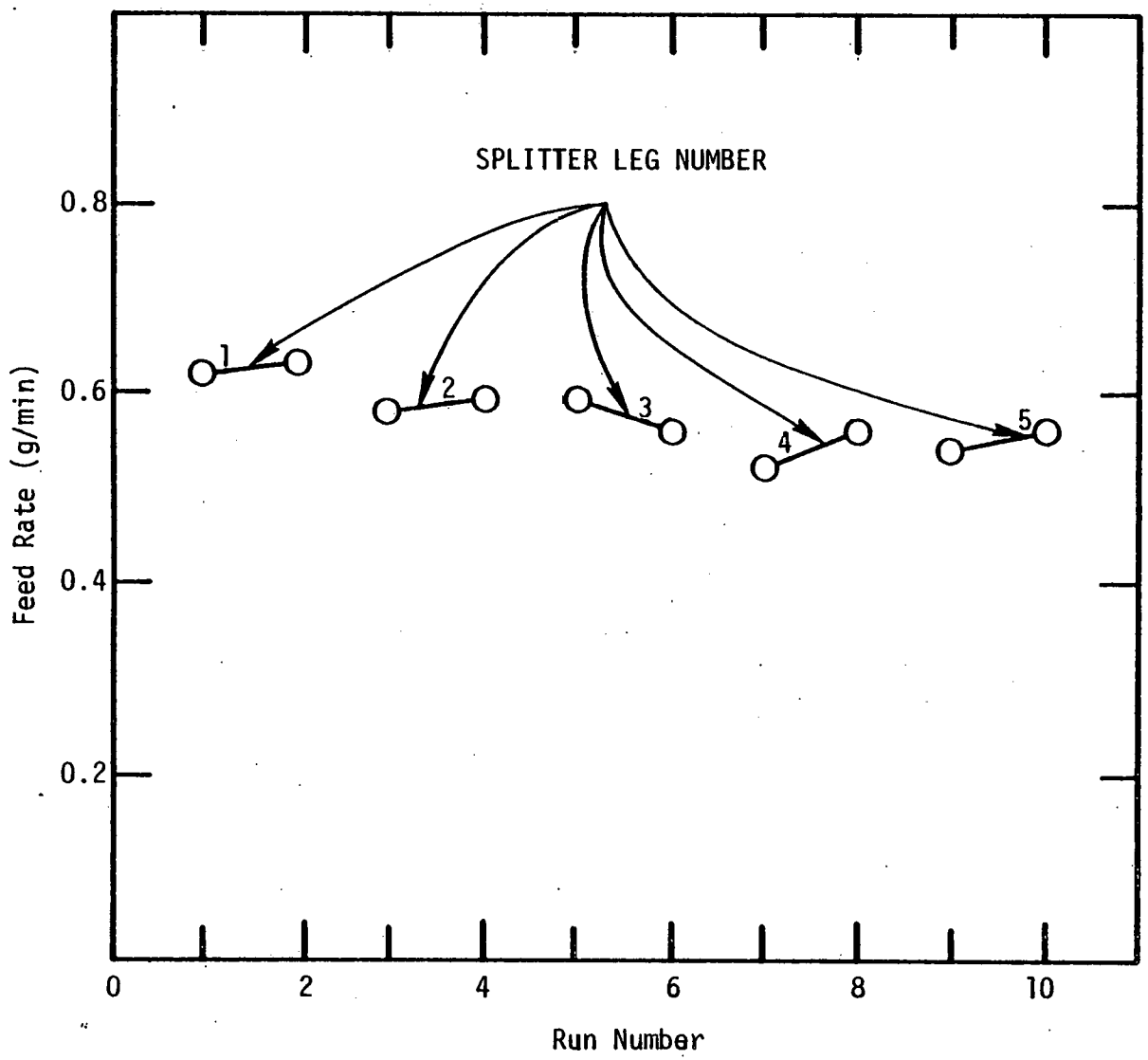

Figure 3-4. Stream Splitter Tests.

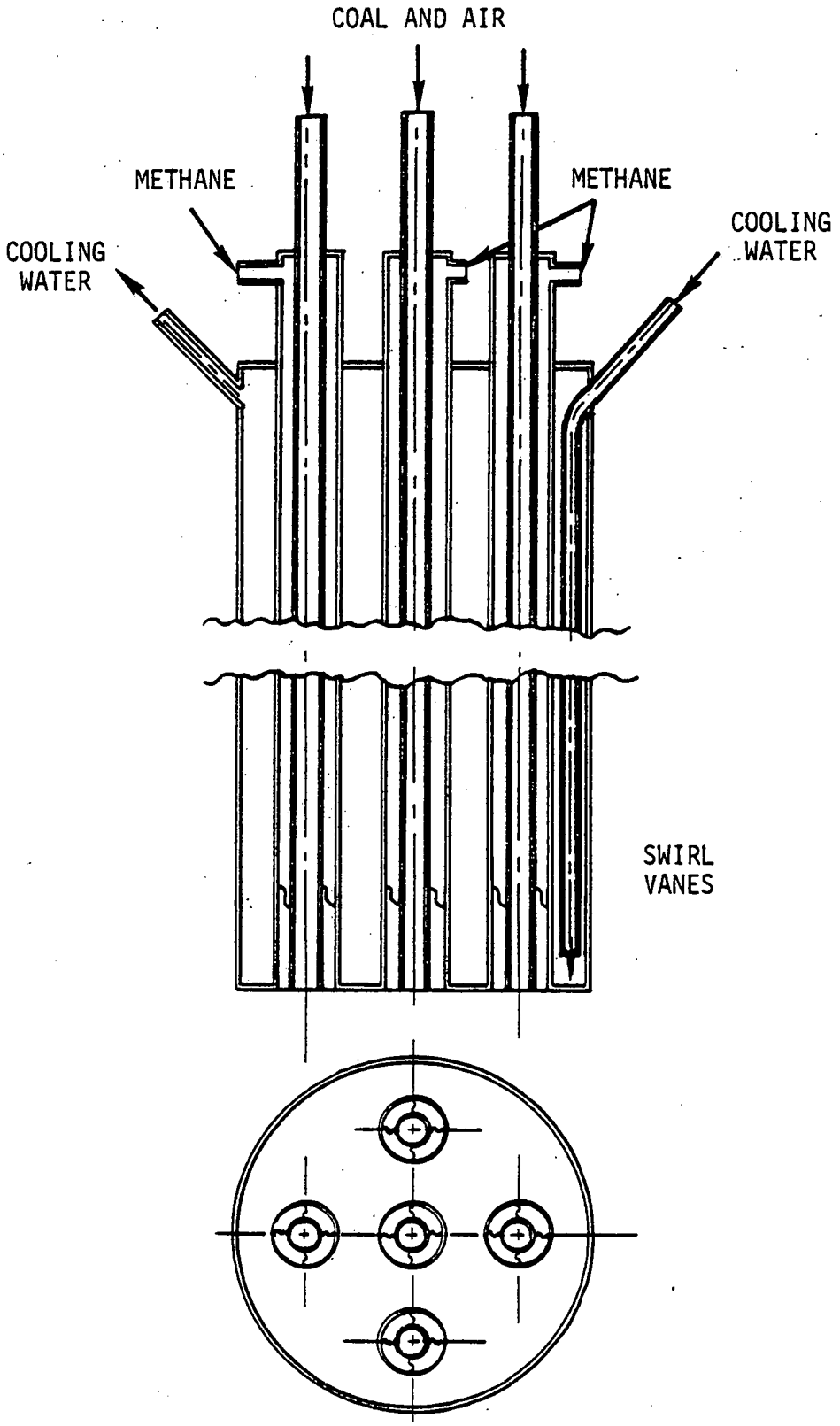

Figure 3-5. Multiple Injector Burner.

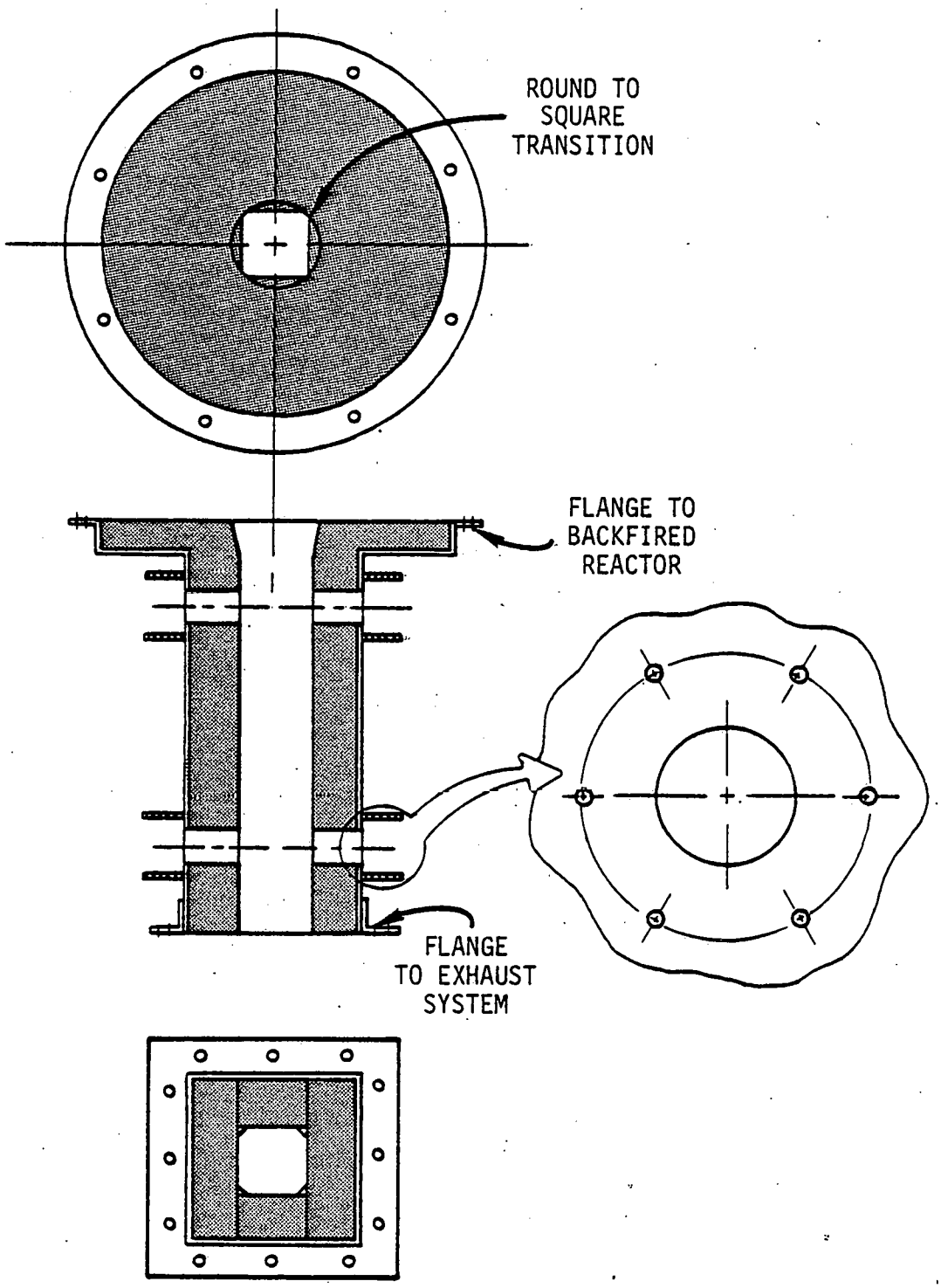

Figure 3-6. Access Module.

of the opposing sides contain round flanges to hold 25 mm diameter infrared windows (Z_nS_e) or collimating probes aligned to provide a clear optical path through the reactor. The remaining two sides contain rectangular flanges to house larger glass windows for visual access. The module is flanged to connect on the top to the backfired reactor or burner adaptor and to connect on the bottom to the exhaust system.

3.3 Measurement System

The measurement system provides for a variety of optical and extractive measurements. Optical instrumentation includes a narrow-angle spectral radiometer, a high-speed camera, and a laser-doppler anemometer.

The radiometer, shown schematically in Figure 3-7, provides a measure of the extinction coefficient of the particulate cloud within its narrow field of view. In the complete system, radiation from an infrared source is focused and passed through the hot particulate stream into a blackened cold-wall collimating probe. Radiation exiting the probe is focused and split into seven narrow beams which pass through narrow-band filters, chosen to avoid combustion gas absorption bands, into solid state infrared radiation detectors. The signal of each of the detectors is amplified, passed into a rapid-switching multiplexer, converted to a digital signal, and is reduced by a Digital 11/23 computer. Table 3-1 lists the detectors, filter wavelengths, and equivalent noise levels for a 20 microsecond sample time, corresponding to a 140 second cycle time. Because the residence time of a single particle in the field of view is approximately 1 millisecond, this rapid switching capability allows a complete spectral sweep to be taken of an essentially frozen particulate cloud. Thus intensities at different wavelengths can be compared, even in a rapidly changing combustion environment, allowing the development of a spectral profile of radiation intensity and the measurement of particle temperature by two-color pyrometry. Choppers located between the source and the reactor and between the reactor and the detector allow alternating measurement of background radiation, flame radiation, and source radiation through the flame. Optics are provided to occasionally measure source radiation alone and to calibrate the system against a blackbody source.

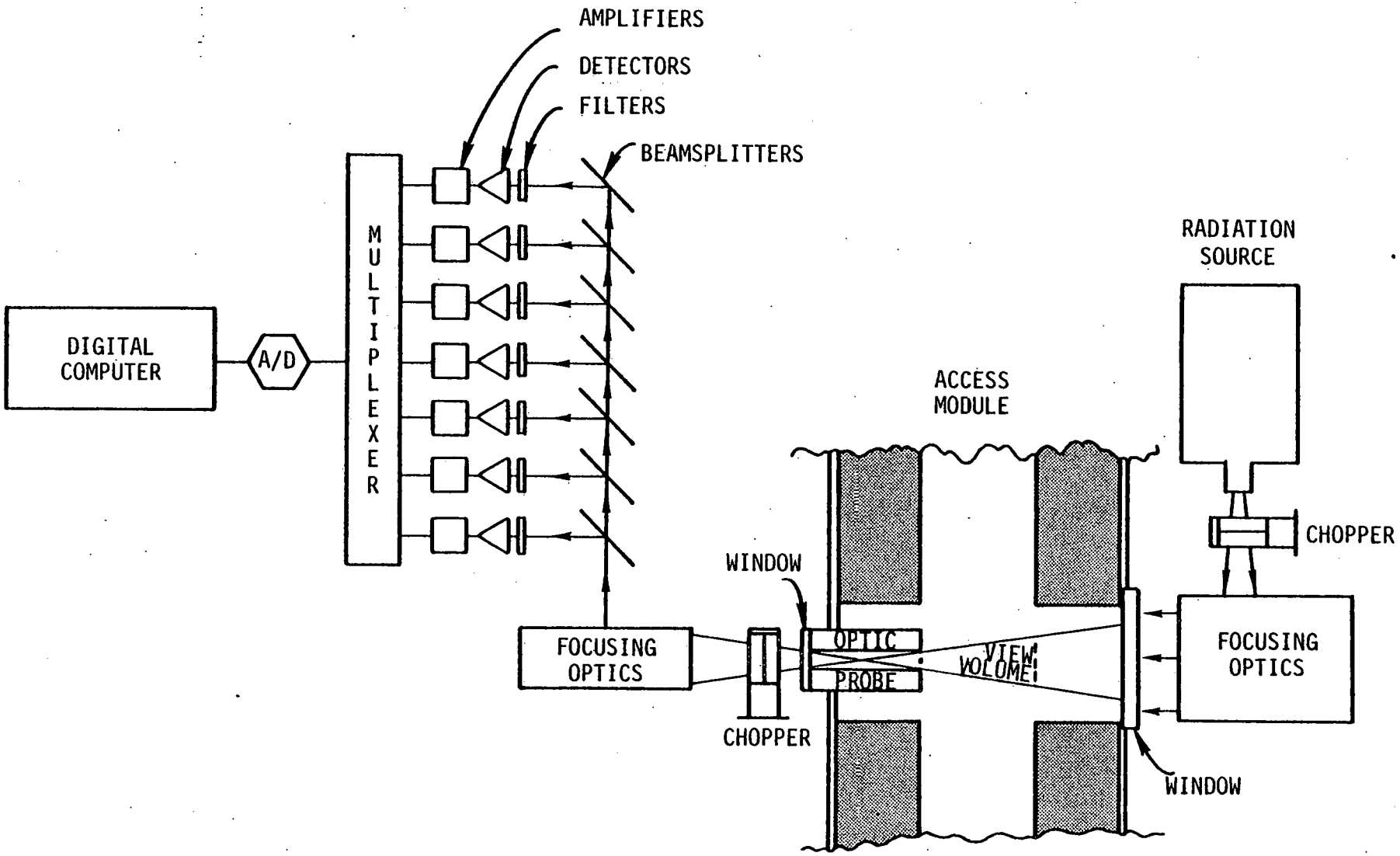

Figure 3-7. Radiometer System.

Table 3-1. Noise Equivalent Power of Selected Detector/Filters.

Detector (type)	Filter		Noise Equivalent Power @ 50 KHz (watts)
	Wavelength (microns)	Bandwidth (microns)	
Silicon	0.75	0.01	3.0×10^{-12}
Silicon	0.95	0.01	2.8×10^{-12}
Lead Sulfide (-30C)	2.20	0.09	8.5×10^{-11}
Lead Selenide (-30C)	3.60	0.13	1.3×10^{-9}
Lead Selenide (-30C)	5.10	0.15	1.0×10^{-9}
Pyroelectric	11	6	6.7×10^{-8}
Pyroelectric	None		6.7×10^{-8}

With these measurements, at a particular wavelength λ, the extinction coefficient b, a measure of the proportion of incident radiation not transmitted through a particulate cloud of length L as defined by

$$dI = - bI\, d\ell \quad , \qquad \left(\text{Friedlander}^{(21)}\right)$$

where I is radiation intensity, can be calculated:

$$b_\lambda = - L\, \ell n \left(\frac{\text{I source through flame - I flame}}{\text{I source}} \right)_\lambda$$

where the extinction coefficient is the sum of the scattering and absorption coefficients:

$$b_\lambda = b_\lambda \text{ scattering} + b_\lambda \text{ absorption.}$$

High-speed photographs, taken through the large rectangular glass windows of the access module, allow observation of the general physical behavior of particles during combustion. This includes in-situ optical measurement of the size of larger particles and qualitative observation of volatile emission and soot formation.

Laser-doppler anemometry, planned for the detailed studies, provides an in-situ measurement of particle velocity and size. The velocity of a particle can be calculated from the frequency of modulation of the intensity of a signal caused by the interference of two coherent (split laser) light beams one of which has been scattered by the moving particle causing a doppler shift in its frequency. The size of the particle is related to its visibility, the ratio of the difference to the sum of the maximum and minimum intensities of the interference fringes as explained by Farmer.[20]

Extractive particle samples are taken isokinetically through an asially mobile porous-wall probe shown in Figure 3-8. This probe, similar to the one used by Mims et al (24), passes two constant streams of inert gas through the porous walls which cools the sample, quenches all reactions, and prevents particle deposition to the wall due to diffusion, turbulent deposition, and thermophoresis. A high flow of inert gas is introduced near the probe tip where rapid quenching is desired and high velocities are necessary to overcome high thermophoretic forces; and a much lower flow of inert gas is introduced to prevent deposition along the length of the probe.

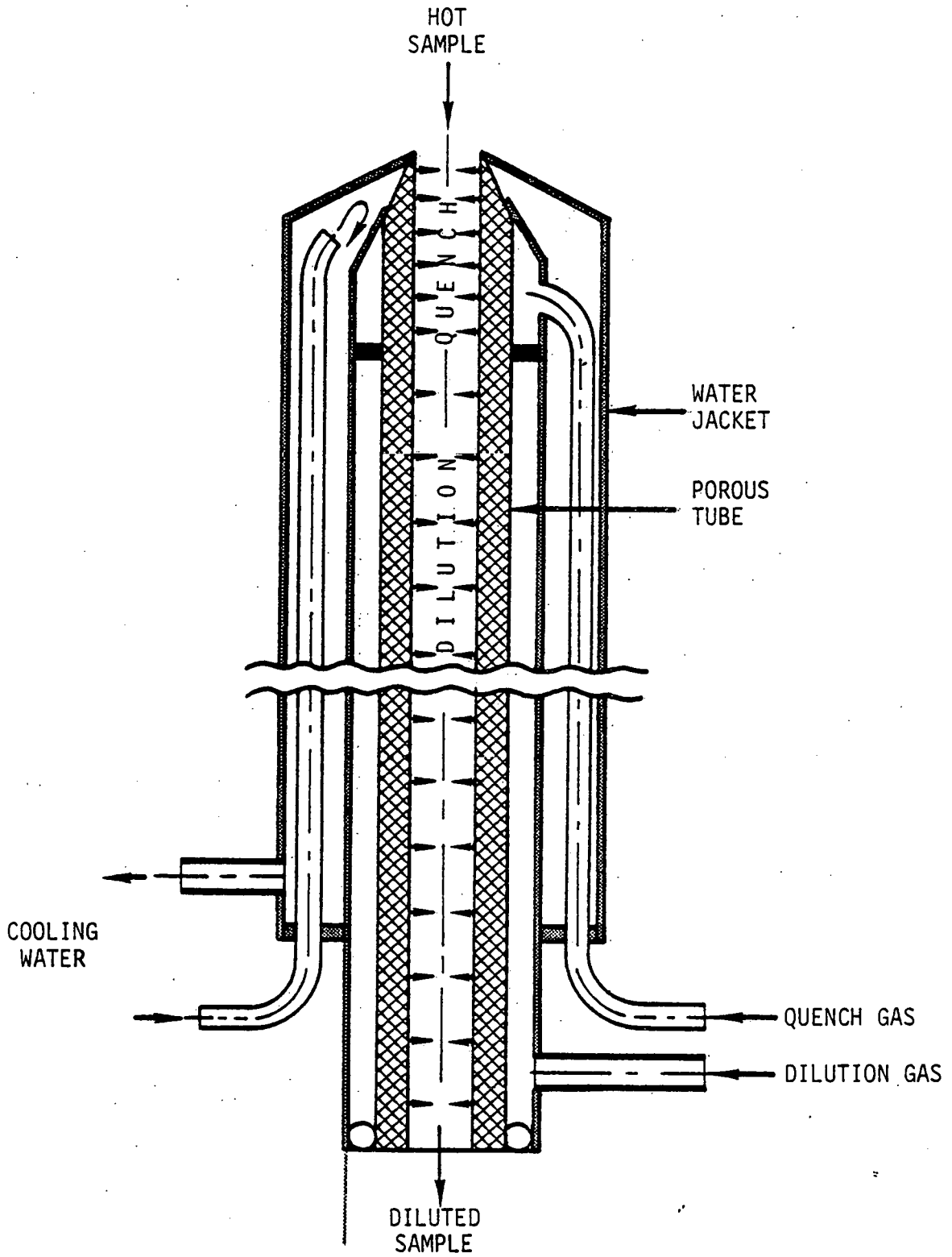

Figure 3-8. Porous Wall Particle Probe.

Extractive measurements of particle size distribution are taken by scanning electron micrographs of nucleopore filter samples, by cascade impactor, and by Malvern laser diffraction. Comparison of optical diameter (SEM, Malvern) with aerodynamic diameter (impactor) provides a measure of particle density. Chemical analysis can be performed on impactor samples and on nucleopore filter samples to differentiate between organic (soot, char, coal) and inorganic (fly ash) particulate.

Size distribution is an important parameter in the determination of the extinction coefficient b of a cloud of spherical particles of uniform density:

$$b = 1.5 \frac{fm}{\rho_p} \int_0^1 \frac{KdM}{X} \qquad \left(\text{Sarofim and Hottel}^{(25)}\right)$$

where fm is the mass of particles per unit volume of space, ρ_p is the particle density, M is the mass fraction of particles of diameter greater than X, and K is the particle extinction efficiency, a function of the wavelength, particle size, and complex index of refraction. By measuring the concentration, density, and size distribution of particulate matter, and by assuming a complex index of refraction based on literature values for soot, char, coal, and fly ash, K at a given wavelength can be calculated numerically from Mie theory (Hottel and Sarofim[23]) allowing a comparison of b_λ calculated with b_λ measured by the radiometer.

Extractive gas samples are taken through a water-cooled probe. Instrumentation is available to continuously monitor O_2 by paramagnetic analysis, CO_2 and CO by infrared absorption, NO by chemiluminescence, and total hydrocarbons by flame ionization. In addition, batch samples can be taken and subsequently analyzed for H_2O, NH_3, HCN, and specific hydrocarbons.

3.4 Exhaust System

Combustion exhaust and backfired exhaust are cooled by dilution and drawn outside the laboratory by a high-pressure blower. Butterfly valves on the inlet and outlet ducts for each system allow independent control of dilution flow and combustor and backfired reactor pressure.

4.0 REFERENCES

1. Richter, W., W. Clark, R. Payne. Assessment of Pulverized Coal Fired Combustor Performance. Contract No. DE-AC22-80PC30297. First Quarterly Technical Progress Report, January 1981.

2. Richter, W. and M. P. Heap. A Semistochastic Method for the Prediction of Radiative Heat Transfer in Combustion Chambers. Western States Section, The Combustion Institute, 1981 Spring Meeting, Paper 81-17.

3. Richter, W. Models for Coal Combustor Performance. Analytical Tool Verification. Topical Report. Prepared for Pittsburgh Energy Technology Center, Department of Energy Under Contract No. DE-AC22-80PC30297, February 1981.

4. Bauersfeld, G.: Weiterentwicklung des Zonenverfahrens zur Berechnung des Strahlungsaustausches in technischen Feuerungen. Dissertation, Universität Stuttgart 1978.

5. Richter, W., G. Fleischhans, C. V. S. Murty. Prediction of Radiative Heat Transfer in a Heavy Fuel Oil Flame. Joint Meeting of the Heat and Gas Transfer Panels, IFRF, November 1978. Doc. No. F24/ga/21.

6. Michel, J. B., and R. Payne. Detailed Measurement of Long Pulverized Coal Flames for the Characterization of Pollutant Formation. Subcontract EER 8318, IFRF Doc. nr. F09/a/23, May 1980.

7. Johnson, T. R., and Beér, J. M. The Zone Method Analysis of Radiant Heat Transfer: a Model for Luminous Radiation. J. Inst. Fuel, 46, 1973, 388.

8. Hottel, H. C., and A. F. Sarofim. Radiative Transfer. McGraw-Hill Book Company. 1967.

9. Sarofim, A. F., and H. C. Hottel. Radiative Transfer in Combustion Chambers: Influence of Alternative Fuels. Proc. of 6th Int. Heat Transfer Conference, Vol. 6, pp. 199-217, Hemisphere Publishers, Washington 1978.

10. Richter, W. and M. P. Heap. The Impact of Heat Release Pattern and Fuel Properties on Heat Transfer in Boilers. Paper prepared for the 1981 ASME Winter Annual Meeting.

11. Lowe, A., McC. Stewart and T. F. Wall. The Measurement and Interpretation of Radiation from Fly Ash Particles in Large Pulverised Coal Flames. 17th Symposium (Int.) on Combustion, The Combustion Institute, 1979. pp. 105-113.

12. Wall, T. F., A. Lowe, L. J. Vibberley, and I. McC. Stewart. Mineral Matter in Coal and the Thermal Performance of Large Boilers. Prog. Energy Combust. Sci., Vol. 5, 1979. pp. 1-29.

13. Wall, T. F., A. Lowe, L. J. Wibberley, T. Mai-Viet, R. P. Gupta. Fly Ash Characteristics and Radiative Heat Transfer in Pulverised-Coal-Fired Furnaces. Dept. Chem. Engineering, The University of Newcastle, N.S.W. 2308, Australia, 1980.

14. Steward, F. R., and K. H. Gürüz. The Effect of Solid Particles on Radiative Transfer in a Cylindrical Test Furnace. Fifteenth Symposium (International) on Combustion. The Combustion Institute, 1975. pp. 1271-1283.

15. Field, M. A., D. W. Gill, B. B. Morgan, and P. G. W. Hawksley. Combustion of Pulverized Coal. The British Coal Utilization Research Association, Leatherhead, Surrey, England. 1967. p. 229.

16. Hemsath, K. H. Zur Berechnung der Flammenstrahlung. Dissertation, University Stuttgart, West Germany, June 1969.

17. A. Blokh. The Problem of Flame as a Disperse System. Heat Transfer in Flames. Scripta Book Company, Washington, D.C., Chapter 6. 1974.

18. Smoot, L. D., and D. T. Pratt. Pulverised-Coal Combustion and Gasification. Plenum Press, New York and London. 1979.

19. Flagan, R. C. Submicron Particles from Coal Combustion. 17th Symposium (Int.) on Combustion, The Combustion Institute, 1979. pp. 105-113.

20. Farmer, N. M.: Applied Optics, 11 2603 (1972).

21. Friedlander, S. K.: Smoke, Dust and Haze, p. 139, Wiley-Interscience, N.Y. (1967).

22. Hamor, R. J., and I. W. Smith: Fuel, 50, 394 (1971).

23. Hottel, H. C., and A. F. Sarofim: Radiative Transfer, p. 398, McGraw-Hill, N.Y. (1967).

24. Mims, C. A., M. Neville, R. J. Quann, and A. F. Sarofim: "Laboratory Studies of Trace Element Transformations During Coal Combustion," Presented at National 87th AIChE Meeting, Boston (1979).

25. Sarofim, A. F., and H. C. Hottel, Proceedings of the 6th International Heat Transfer Conference, Vol. 6, pp. 199-217, Hemisphere Publishers, Washington (1978).